Design and Performance Analysis of a Modified Proportional Multi-Resonant (PMR) Controller for Three-Phase Voltage-Source Inverters

Ahmad Ali Nazeri, Mahmoud Saeidi, and Peter Zacharias
Centre of Competence for Distributed Electric Power Technology
Faculty of Electrical Engineering / Computer Science
University of Kassel, Kassel, Germany
Email: ahmad.nazeri@student.uni-kassel.de,
{mahmoud.saeidi, peter.zacharias}@uni-kassel.de

August 15, 2022

Acknowledgments

This work was financially supported by the German Academic Exchange Service (DAAD) Germany and providing fully funded scholarship to Ahmad Ali Nazeri to support his doctoral studies.

Keywords

≪Current control≫, ≪Discretization≫, ≪Harmonics≫, ≪Non-linear load≫, ≪Resonant control≫

Abstract

The three-phase voltage source inverter (VSI) can be operated in grid-connected and/or stand-alone mode where the VSI is connected to the grid and/or critical loads at the point of common coupling (PCC). Proper voltage control is needed for the output voltage regulation in stand-alone operation and current control is needed for the grid current control. This paper presents a step-by-step design procedure, an extensive system stability analysis, and methods of discretization for the current control of three-phase power converters in the synchronous (dq) and stationary reference frame (SRF). A proportional-integral multi-resonant (PI-MR) controller in the synchronous reference frame (SynRF) is implemented for the regulation of the inner current loop. Moreover, the inverter inductor current controller in a stationary frame is proposed to provide active damping, and improve transients, and steady-state performance. The traditional PI-MR controller is compared for different load conditions with the modified practical proportional multi-resonant (PMR) controller in parallel with the harmonic compensators of orders 5th, 7th, 11th, and 13th to reduce low-order load current harmonics. The PMR controller shows superior performance with lower total harmonic distortion (THD) than the conventional PI and PI-MR controllers for highly nonlinear load conditions. Moreover, the modified PMR controller has almost zero steady-state error, improved tracking of the reference signal, and better disturbance rejection compared to the conventional PI-MR control. A comprehensive design guideline of the proposed controller with a wider range of system stability margin is analyzed with harmonic damping of the three-phase VSI. Proper discretization methods for each controller have been outlined. The system is simulated in MATLAB/Simulink environment and experimentally implemented on a TMS320F28335 floating-point digital signal processor (DSP) for a 7.5 kW inverter to validate the performance of the controllers.

Introduction

The distributed generation (DG) systems such as photovoltaic (PV), wind energy, and fuel cell are extensively integrated with the power electronic converters [1].

The voltage source inverters (VSIs) are widely interfaced in different power conversion applications such as island mode (microgrids), distributed generation, shunt active filters, and uninterruptible power supplies (UPS) [1]. Normally, the pulse-width-modulation (PWM) inverters can be operated in stand-alone and/or grid-connected mode [2, 3]. A constant voltage constant frequency (CVCF) PWM inverter should be used to regulate the output voltage with low total harmonic distortion (THD) and fast transient performance [4]. In, grid-connected mode, a fast current controller must be able to inject a nearly sinusoidal current into the grid with low THD according to the IEEE standards [5]. The three-phase VSI can be connected to the grid and/or the load at the point of common coupling (PCC). A voltage and current controller is needed for the output voltage and grid current regulation when the three-phase VSI is connected in stand-alone feeding loads or grid-connected injecting the grid current [6]. The basic working principle of PWM VSI is to convert the dc voltage to a sinusoidal ac output connected with an *LC* filter. The performance of the VSI is evaluated by the content of THD, the transient response, and overall efficiency [6]. The rectifier loads connected at the point of PCC affect the output current and voltage and introduce distortions into the output of the PWM VSI, which degrades the power quality [2]. The objective of a control system for the three-phase VSI system is to keep the output current nearly sinusoidal with minimum zero steady-state error and low THD under rectifier load [7].

To address this problem, there is a need for a current controller, which improves the dynamic and transient performance of the system, offers a wide range of stability margins, and provides almost zero steady-state error [8]. Several control strategies in the literature have been reported such as conventional proportional-integral (PI) control [9], proportional-resonant (PR) control [10], repetitive control (RC) [11], deadbeat model and predictive control [12]. The RC based on the internal model principle [11], perfectly tracks the periodic reference, eliminating the periodic errors from the rectifier loads. The RC is normally combined with another feedback controller or a deadbeat controller to improve the system stability, which increases the complexity and tuning of the controller [13]. Moreover, the RC uses large memory and has a slow response to non-periodic disturbance [13]. The traditional PI control is simple to implement but it has a steady-state error with poor tracking capability and poor disturbance rejection. On the other hand, the PR control eliminates the zero steady-state error, better tracking of the reference signal, and has better disturbance rejection [7]. The PI control in SynRF (dq) is identical to the ideal PR control in SRF ($\alpha\beta$) [10]. The PI control in the SynRF combined with the multiple resonant control (MR) in the SRF namely PI-MR can be used in current control to reduce the harmonics introduced by the rectifier loads [14].

This paper presents a modified practical proportional multiple-resonant (PMR) current control in parallel with the harmonic compensators (HCs) of orders 5th, 7th, 11th, and 13th used to mitigate the low-order load current harmonics. Moreover, a step-by-step design procedure of the PMR current control with the analysis of system stability is presented. A wide range of stability margins for the current control is derived based on the design methodology. The dynamic and transient performance of the modified PMR current control is compared with the traditional PI-MR for highly nonlinear loads. Also, the proper discretization methods for the PI-MR and PMR controllers are derived for the practical implementation of the controller on TMS320F28335 32-bit floating-point digital signal processor (DSP). The modified PMR controller can also be implemented in the voltage control in stand-alone operation and/or grid-current control for grid-connected mode. The proposed methodology is simulated in MATLAB/Simulink environment and experimentally implemented on a 7.5 kW three-phase VSI, which effectively tracks the reference signal with nearly zero steady-state error and reduces the output current THD.

Harmonic Damping Scheme for Three-Phase VSI System

Fig. 1 shows the block diagram of a three-phase VSI with an *LC* filter. The dc-ink voltage V_{dc} is assumed to be constant. The inverter is connected to an *LC* filter L_f, C_f, and the load Z_L. R_f is the equivalent series resistance (ESR) of the filter inductance L_f. i_L, i_c, and i_o are the inverter, capacitor and load currents respectively where v_o is the output voltage. The reference rectifier load is connected with the load resistance R_d as depicted in Fig. 1. The system parameters are given in Table I. The traditional PI controller in SynRF (dq) can be used to regulate the output current of the inverter [14]. The three-phase output currents are transformed to the dq frame and given to the PI controller as shown in Fig. 2.

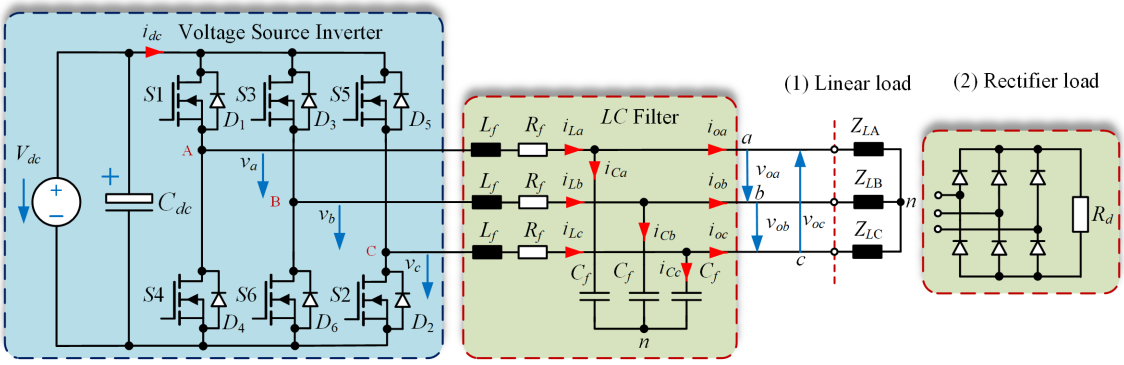

Fig. 1: Diagram of a three-phase VSI with an *LC* filter

The standard PI controller is given in (1a) forces the error in the dq axis to zero and decouples the d and q components. This control scheme is similar to the ideal PR controller in $\alpha\beta$ frame [16] given in (1b). The ideal PR controller has an infinite gain at the nominal grid frequency ω_o [8], has no phase shift and gain at other frequencies [16], and has a better tracking capability of AC reference signals compared to the PI control [10]. A multi-resonant (MR) controller in $\alpha\beta$ frame given in (1c) can be used in parallel to the standard PI controller in dq frame to compensate for the harmonics in the load current when a highly non-linear load is connected as shown in Fig. 2. The traditional PI with the MR control scheme is referred as PI-MR controller as depicted in Fig. 2. The transfer functions of each controller is expressed as

$$G_{\mathrm{PI},ci}(s) = K_{pi} + \frac{K_{i1}}{s} \tag{1a}$$

$$G^{s}_{\mathrm{PR},ci}(s) = K_{pi} + \frac{K_{i1}s}{s^2+\omega_o^2} \tag{1b}$$

$$G^{s}_{\mathrm{MR},ci}(s) = \sum_{n=1}^{k} \frac{K_{in}s}{s^2+(n\omega_o)^2} \tag{1c}$$

$$G^{s}_{\mathrm{PMR},ci}(s) = K_{pi} + \frac{K_{i1}\omega_d s}{s^2+2\omega_d s+\omega_o^2} + \sum_{n=1}^{k} \frac{K_{in}\omega_d s}{s^2+2\omega_d s+(n\omega_o)^2}. \tag{1d}$$

Table I: System parameters

Parameter	Symbol	Value	Unit
Nominal active power	$P_{\max}$	7.5	[kW]
Base voltage	V_B	325	[V]
Base current	I_B	15.3	[A]
Base impedance	Z_B	21.3	[Ω]
Base capacitance	C_B	150	[μF]
DC input voltage	V_{dc}	400	[V]
Nominal frequency	f_o	50	[Hz]
Switching frequency	f_{sw}	20	[kHz]
Sampling time	T_s	50	[μs]
PWM Time delay	T_d	75	[μs]
Filter inductance	L_f	2.6	[mH]
Filter winding resistance	R_f	0.1	[Ω]
Filter capacitance	C_f	6	[μF]
Connected load	R_d	12.74	[Ω]

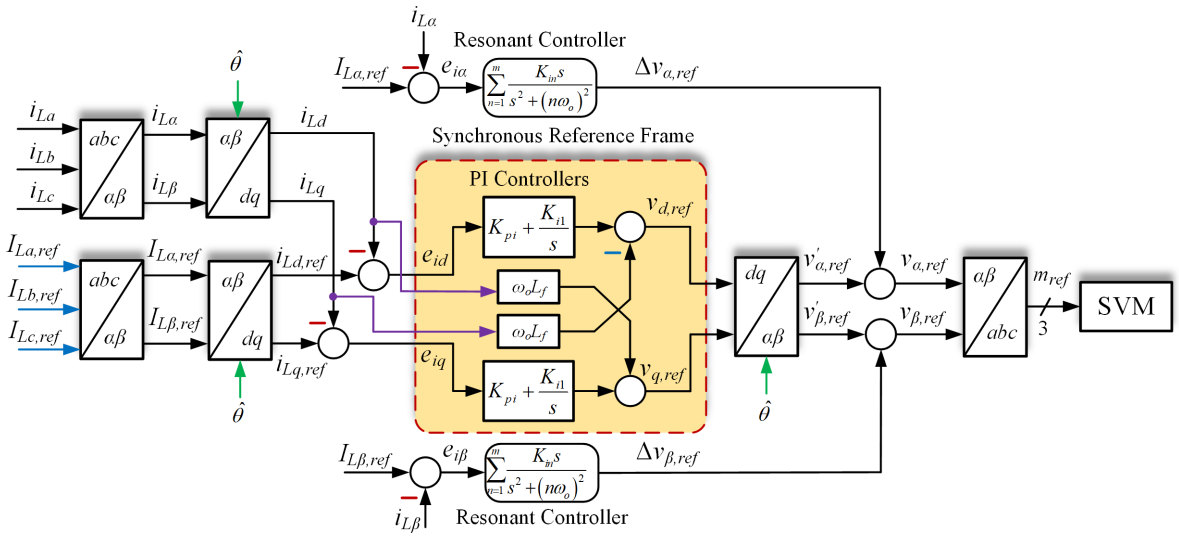

Fig. 2: Control structure of the standard PI with multi-resonant (MR) current control

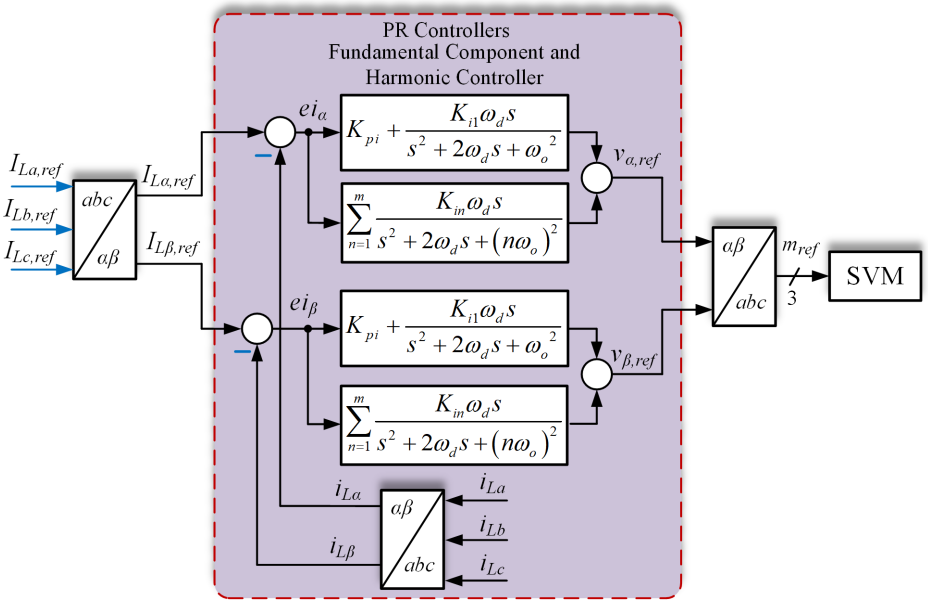

Fig. 3: Control block diagram of the practical proportional multi-resonant (PMR) current control

where 's' denotes the αβ-frame. K_{pi} is the proportional gain, K_{i1} and K_{in} are the fundamental and multiple harmonic integral gains. n denotes the harmonic order, ω_o is the fundamental grid frequency, and ω_d is the cut-off frequency of the PMR controller. The modified PMR current control in αβ frame given in (1d), which has a finite gain at the target frequency, has better transient performance, and is capable to regulate the output current close to the reference signal compared to the traditional PI and PI-MR controllers [15]. However, there is a trade-off between the damping ratio ω_d for stable a operation and the controller gains at the selected frequency to force the zero steady-state error [13]. Choosing smaller ω_d makes the filter more sensitive to the frequency variations, leads to slow transient response [13], and makes it difficult for the practical implementation of the DSP due to its deteriorating performance and limited resolution [17]. The modified PMR controller has half of the resonance gain proposed in [10, 16] and harmonic compensating terms are normally added in parallel to the fundamental controller for the excellent harmonic damping capability with fast transient performance as shown in Fig. 3.

Controllers Design

Design Procedure of the PI Current Control

The standard PI current control given in (1a) is taken with the transport and sampling delay e^{-sT_d} in the forward path and the plant illustrated in Fig. 4, which gives the open-loop transfer function of the current control as

$$G_{\mathrm{OL},ci}(s) = \underbrace{K_{pi}\left(1+\frac{K_{i1}}{sK_{pi}}\right)}_{\text{PI current controller}} \underbrace{\left(e^{-sT_d}\right)}_{\text{PWM delay}} \underbrace{\left(\frac{K_f}{sT_f+1}\right)}_{\text{Inverter}}. \tag{2}$$

where T_d is the combined sampling and transport delay times, $K_f = V_{dc}/R_f$, and $T_f = L_f/R_f$ are the plant transfer functions. Substituting $s \to j\omega_{ci}$ in (2) and applying the Nyquist stability criterion such as when the phase response reaches $-\pi$, the magnitude response must be less than 1 to ensure no encirclement of the -1. Deriving the open-loop magnitude and phase response of the forward current loop at the cross-over frequency ω_{ci} [18]

$$\begin{aligned}
\angle G_{\mathrm{OL},ci}(j\omega_{ci}) &= \angle\left\{\left[K_{pi}\left(1+\frac{K_{i1}}{j\omega_{ci}K_{pi}}\right)\right]\times e^{-j\omega_{ci}T_d}\times\left(\frac{K_f}{j\omega_{ci}T_f+1}\right)\right\}\\
&= (-\pi+\phi_m)\\
&\approx \tan^{-1}\left(\frac{\omega_{ci}K_{pi}}{K_{i1}}\right)-\frac{\pi}{2}-\omega_{ci}T_d-\tan^{-1}(\omega_{ci}T_f).
\end{aligned} \tag{3}$$

At ω_{ci}, the phase contribution of $\tan^{-1}(\omega_{ci}K_{pi}/K_{i1}) \approx \pi/2$ and $\tan^{-1}(\omega_{ci}T_f) \approx \pi/2$. Therefore, the maximum crossover frequency $\omega_{ci,\max}$ can be written as [17]

$$\omega_{ci,\max} = \frac{\pi/2-\phi_m}{T_d}. \tag{4}$$

The maximum magnitude of K_{pi} can be found by setting the (3) as $|G_{\mathrm{OL},ci}(j\omega_{ci,\max})| = 1$ which gives,

$$K_{pi} = \left(\frac{\omega_{ci,\max}K_{pi}}{K_{i1}K_f}\right)\frac{\sqrt{1+\omega_{ci,\max}^2T_f^2}}{\sqrt{1+\frac{\omega_{ci,\max}^2K_{pi}^2}{K_{i1}^2}}}. \tag{5}$$

Considering $\omega_{ci,\max}K_{pi}/K_{i1} >> 1$ and $\omega_{ci,\max}T_f >> 1$. Substituting K_f and T_f in (5) with simplification, which results in the proportional gain K_{pi} as [18],

$$K_{pi} = \frac{\omega_{ci,\max}T_f}{K_f} = \frac{\omega_{ci,\max}L_f}{V_{dc}}. \tag{6}$$

The integral gain K_{i1} can be determined by setting $\tan^{-1}(\omega_{ci,\max}K_{pi}/K_{i1}) \approx \pi/2$,

$$K_{i1} = \frac{\omega_{ci,\max}K_{pi}}{\tan 89.1^\circ} = \frac{\omega_{ci,\max}K_{pi}}{30}. \tag{7}$$

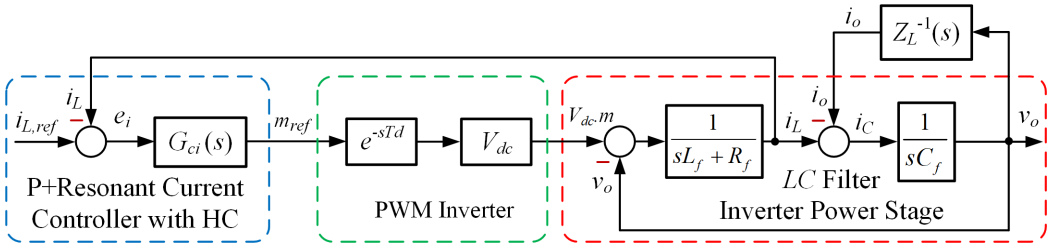

Fig. 4: Closed loop control structure of the system in the stationary reference frame

Design Procedure of the PMR Current Control

The open-loop transfer function of the PMR current control in αβ frame shown in Fig. 4 and is expressed as

$$G^s_{\mathrm{OL},ci}(s) = \underbrace{\left(K_{pi} + \frac{K_{i1}\omega_d s}{s^2+2\omega_d s+\omega_o^2}\right)}_{\text{PMR current controller}} \underbrace{\left(e^{-sT_d}\right)}_{\text{PWM delay}} \underbrace{\left(\frac{K_f}{sT_f+1}\right)}_{\text{Inverter}}. \tag{8}$$

where ω_d limits the forward gain at ω_o to $G^s_{\mathrm{PMR},ci}(s) = K_{pi} + K_{i1}/\omega_{ci}$ with the approximation that the cross-over frequency ω_{ci} is much greater than the ω_o, the phase angle of the $G_{\mathrm{OL},ci}(s)$ in (8) can be approximated as [18]

$$\begin{aligned}
\angle G_{\mathrm{OL},ci}(j\omega_{ci}) &= \angle\left\{K_{pi}\left[1+\frac{K_{i1}}{K_{pi}}\times\frac{j\omega_{ci}}{(\omega_o^2-\omega_{ci}^2)+j\omega_{ci}\omega_d}\right]\times e^{-j\omega_{ci}T_d}\times\left(\frac{K_f}{j\omega_{ci}T_f+1}\right)\right\} \\
&= (-\pi+\phi_m) \\
&\approx \tan^{-1}\left(\frac{\omega_{ci}K_{pi}}{K_{i1}}\right) - \frac{\pi}{2} - \omega_{ci}T_d - \tan^{-1}(\omega_{ci}T_f).
\end{aligned} \tag{9}$$

which gives the phase margin as

$$\omega_{ci} = \frac{\tan^{-1}(\omega_{ci}K_{pi}/K_{i1}) - \phi_m}{T_d}. \tag{10}$$

From (10), the maximum cross-over frequency $\omega_{ci,\max}$ for a given phase margin ϕ_m with the approximation of $\tan^{-1}(\omega_{ci,\max}K_{pi}/K_{i1}) \approx \pi/2$, which results in similar results given in (4). The K_{pi} and K_{i1} parameters can be found in similar manner as described in the section of standard PI control design with the approximations. Therefore, the fundamental component parameters are of K_{pi} and K_{i1} given in (6) and (7) can be used respectively. The integral gain of the MR control is designed based on the K_{i1} as $K_{in} = K_{i1}/n$. The current controller is designed in the αβ frame based on (1) used in the open-loop transfer function $G^s_{\mathrm{OL},ci}(s)$ which is written as

$$G^s_{\mathrm{OL},ci}(s) = G^s_{ci}(s) \times e^{-sT_d} \times \frac{K_f}{sT_f+1}. \tag{11}$$

Fig. 5a depicts the comparison of the frequency response of the $G^s_{\mathrm{OL},ci}(s)$ of PI+MR controller (see 1a and 1c) with the PMR+MR controller (see 1d) in the αβ frame extracted from (11). The combined

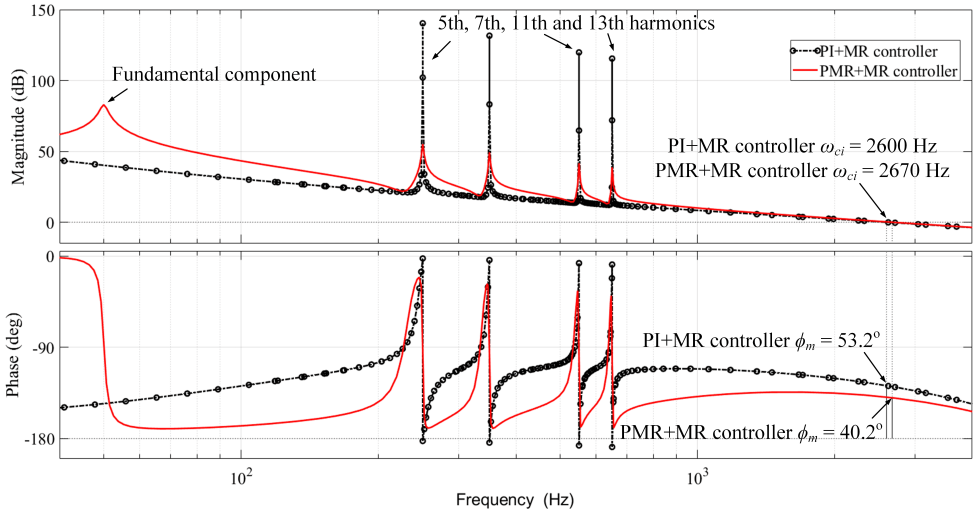

(a)

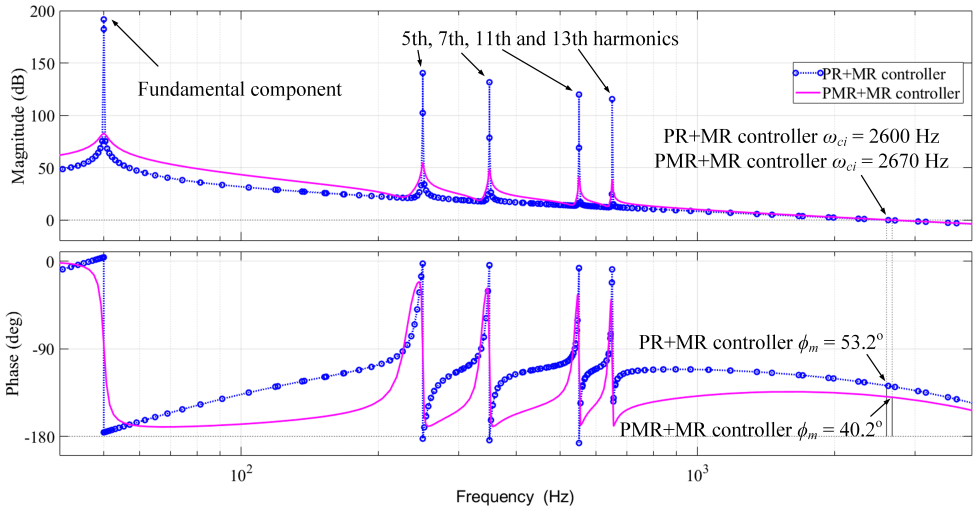

(b)

Fig. 5: Frequency response of the current control loop: (a) open-loop transfer function in synchronous and stationary reference frames of PI+MR and the PMR+MR controllers; (b) open-loop transfer function in stationary reference frame of PR+MR and PMR+MR controllers

sampling and transport delay time is $T_d = 75\mu s$. The set phase margin $\phi_m = 55^o$, and the resulted cross-over frequency $\omega_{ci,\max} = 2 \times \pi \times 2593$ rad/s. However, the final phase margin of the PI+MR controller is slightly reduced to 53.2^o due to the resonance at the output frequency with $\omega_{ci,\max} = 2 \times \pi \times 2600$ rad/s. Fig. 5b presents the comparison of the open-loop frequency response of the PR+MR controller (see 1b and 1c) and PMR+MR controller extracted from (11) where the phase margin $\phi_m = 40.2^o$ is reduced due to presence of the higher-order harmonic controllers with $\omega_{ci,\max} = 2 \times \pi \times 2670$ rad/s [13].

Methods of Discretization

Most of the voltage and current controllers are implemented digitally on a DSP, so the suitable discretization method for the resonant controller should not be ignored [17]. Due to the narrow band and infinite gain of the resonant controller, it is sensitive to the discretization process because the slight displacement in the resonant poles leads to the high loss of controller performance. Moreover, discretization has also an effect on the zeros, as it modifies its displacement with its continuous domain transfer function [17]. The computational delay e^{-sT_d} influences the performance of the system and can lead to system insta-

bility. Hence, the sampling and transport delay has been implemented in the design of the controller. Therefore, great care should be taken while implementing the resonant controllers on DSP [16]. The ideal resonant controller in (1c) is discretized using the forward and backward Euler's method and the PMR controller in (1d) is discretized using the Tustin method.

Forward Euler and Backward Euler Implementation

The results of a MR controller in (1c), when the direct integrator is discretized using the forward Euler $s = \frac{1-z^{-1}}{z^{-1}T_s}$ and the feedback integrator is discretized using the backward Euler $s = \frac{1-z^{-1}}{T_s}$, which results in

$$\begin{aligned} G_{\mathrm{MR},ci}(z) &= \frac{K_{in}\left(\frac{z^{-1}T_s}{1-z^{-1}}\right)}{1+n^2\omega_o^2\left(\frac{T_s}{1-z^{-1}}\right)\left(\frac{z^{-1}T_s}{1-z^{-1}}\right)} = \frac{\left(K_{in}T_s z^{-1}\right)/\left(1-z^{-1}\right)}{\left[\left(1-z^{-1}\right)^2+n^2\omega_o^2T_s^2z^{-1}\right]/\left(1-z^{-1}\right)^2} \\ &= \frac{K_{in}T_s z^{-1}\left(1-z^{-1}\right)}{\left(1-z^{-1}\right)^2+n^2\omega_o^2T_s^2z^{-1}} = \frac{K_{in}T_s\left(z^{-1}-z^{-2}\right)}{1+\left(n^2\omega_o^2T_s^2-2\right)z^{-1}+z^{-2}}. \end{aligned} \tag{12}$$

Comparing (12) to the standard z-domain discrete transfer function in (13) to obtain the coefficients of the MR control and digitally implemented in the direct form II transpose as shown in Fig. 6b and given

$$\frac{Y(z)}{e(z)} = \frac{b_0+b_1z^{-1}+b_2z^{-1}}{1+a_1z^{-1}+a_2z^{-2}}. \tag{13}$$

where $b_0 = 0, \qquad b_1 = K_{in}T_s, \qquad b_2 = -b_1, \qquad a_1 = n^2\omega_o^2T_s^2-2, \qquad a_2 = 1.$

Tustin (trapezoid) Implementation

The results of a PMR controller in (1d) is discretized using Tustin $s = \frac{2}{T_s}\frac{1-z^{-1}}{1+z^{-1}}$ as shown in Fig. 6a and given as [16]

$$\begin{aligned} G_{\mathrm{PMR},ci}(z) &= \frac{K_{in}\omega_d\left(\frac{2}{T_s}\frac{1-z^{-1}}{1+z^{-1}}\right)}{\left(\frac{2}{T_s}\frac{1-z^{-1}}{1+z^{-1}}\right)^2+2\omega_d\left(\frac{2}{T_s}\frac{1-z^{-1}}{1+z^{-1}}\right)+(n\omega_o)^2} \\ &= \frac{(2/T_s)K_{in}\omega_d\left(1-z^{-2}\right)}{(4/T_s^2)\left(1-z^{-1}\right)^2+(4\omega_d/T_s)\left(1-z^{-2}\right)+n^2\omega_o^2\left(1+z^{-1}\right)^2} \\ &= \frac{2K_{in}\omega_dT_s\left(1-z^{-2}\right)}{4\left(1-2z^{-1}+z^{-2}\right)+4\omega_dT_s\left(1-z^{-2}\right)+n^2\omega_o^2T_s^2\left(1+2z^{-1}+z^{-2}\right)} \\ &= \frac{2K_{in}\omega_dT_s\left(1-z^{-2}\right)}{\left(4+4\omega_dT_s+n^2\omega_o^2T_s^2\right)+\left(2n^2\omega_o^2T_s^2-8\right)z^{-1}+\left(4-4\omega_dT_s+n^2\omega_o^2T_s^2\right)z^{-2}}. \end{aligned} \tag{14}$$

To obtain the z-domain discrete transfer function given (13), we divide the nominator and denominator of (14) by temp $= (4+4\omega_dT_s+n^2\omega_o^2T_s^2)$, we get

$$G_{\mathrm{PMR},ci}(z) = \frac{\left(2K_{in}\omega_dT_s/\mathrm{temp}\right)\left(1-z^{-2}\right)}{1+\left[\left(2n^2\omega_o^2T_s^2-8\right)/\mathrm{temp}\right]z^{-1}+\left[\left(4-4\omega_dT_s+n^2\omega_o^2T_s^2\right)/\mathrm{temp}\right]z^{-2}}. \tag{15}$$

where $b_0 = 2K_{in}\omega_dT_s/\mathrm{temp}, \qquad b_1 = 0, \qquad b_2 = -b_0,$
$a_1 = (2n^2\omega_o^2T_s^2-8)/\mathrm{temp}, \qquad a_2 = (4-4\omega_dT_s+n^2\omega_o^2T_s^2)/\mathrm{temp}.$

Fig. 6b depicts the discrete implementation of the modified PMR controller in the direct form II transpose as given in (13) and (15). The difference equation needed for the DSP implementation of the PR controller is given as [16]

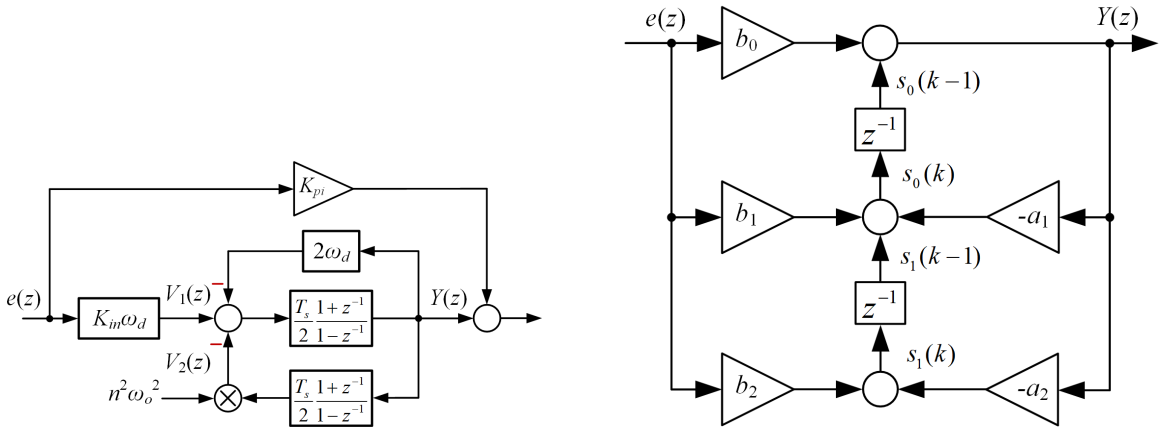

(a) PMR controller (b) Direct form II transpose of modified PMR controller

Fig. 6: Discrete-time implementation of the PMR controller

Table II: Parameters of the current controller

Control schemes	K_{pi}	K_{i1}	$K_{in(5,7,11,13)}$	ω_d [rad/s]	ω_{ci} [rad/s]	ϕ_m
PI-MR	1.37	933.61	186, 133, 84, 71	-	16336	53.2°
PMR-MR	1.78	276.63	55, 39, 25, 21	5	16776	40.2°

$$Y(z) = b_0 e(z) + b_1 e(z) z^{-1} - a_1 Y(z) z^{-1} + b_2 e(z) z^{-2} - a_2 Y(z) z^{-2}. \tag{16}$$

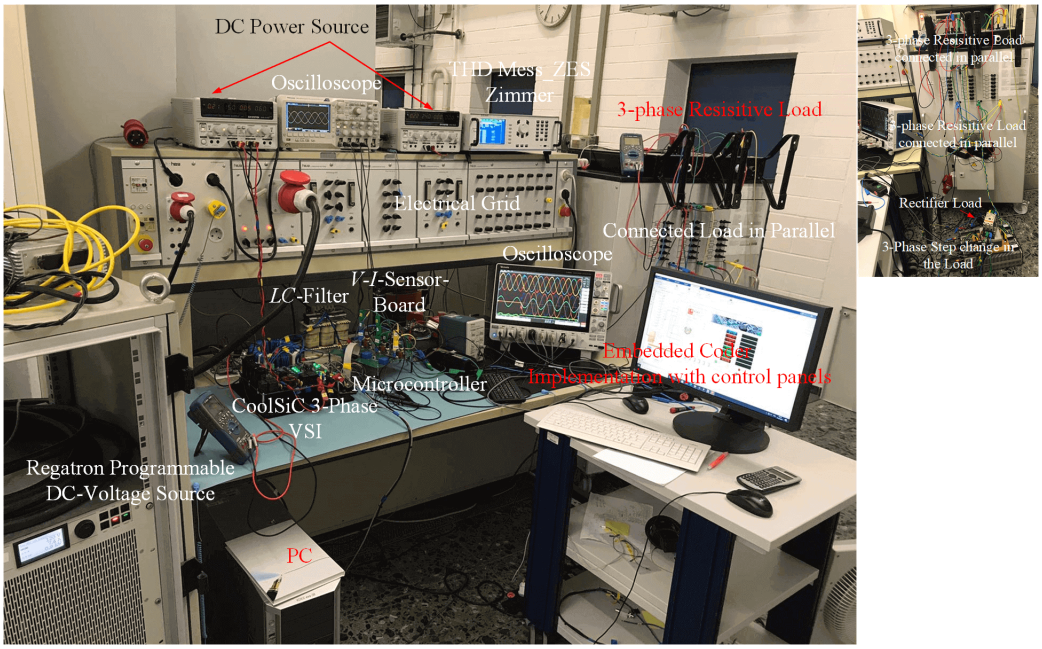

Fig. 7: Experimental prototype of the system

Simulation and Experimental Validations

The three-phase VSI illustrated in Fig. 1 with the control schemes shown in Fig. 2, and 3 were implemented with the space vector modulation (SVM) in MATLAB/Simulink. Fig. 7 shows the experimental setup at the laboratory. The experimental setup includes a constant programmable DC power source

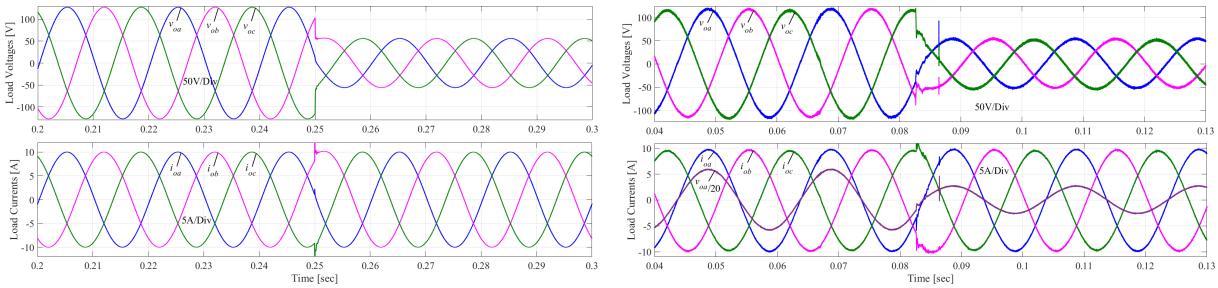

(a) (b)

Fig. 8: Dynamic performance of the three-phase VSI with the step-change in the load employing standard PI control; (a) simulation, (b) experimental

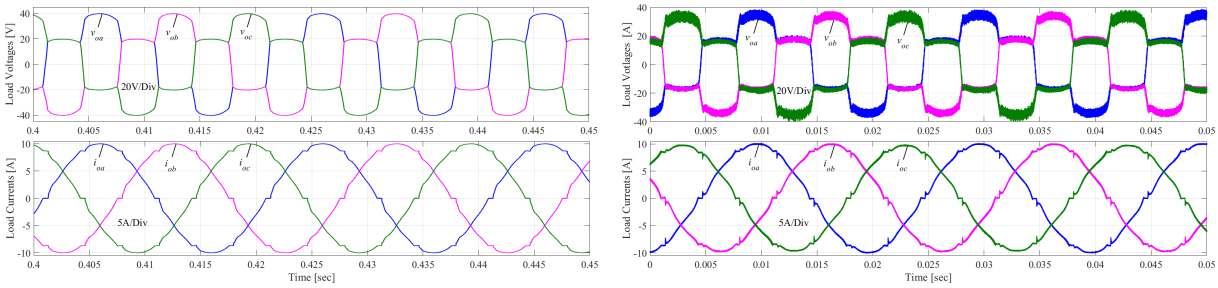

(a) (b)

Fig. 9: The performance of the PI-MR control under highly rectifier load; (a) simulation, (b) experimental

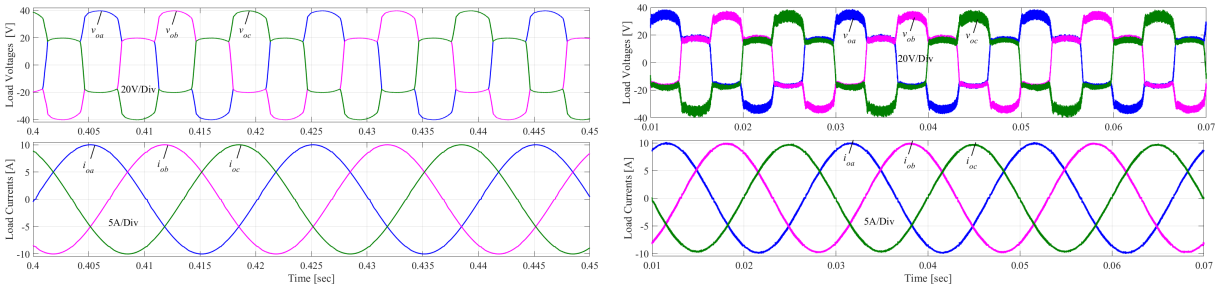

(a) (b)

Fig. 10: The performance of the proposed modified PMR-MR control; (a) simulation, (b) experimental

from Regatron as V_{dc} connected to a three-phase CoolSiC MOSFET of 7.5kW inverter, a three-phase *LC* filter, a three-phase voltage and current sensors, and the load as illustrated in Fig. 7. An 8-channel MSO68B oscilloscope was used to display the results. The current and voltage THDs were extracted from the precision power analyzer ZES-Zimmer. The proposed control schemes were implemented on a 32-bit floating-point TMS320F28335 DSP from Texas Instruments. The sampling was executed in the middle of every sampling period T_s. The base voltage V_B, base current I_B, base impedance Z_B, and the base capacitance C_B given in Table I were used to calculate the control parameters in the per-unit system, and the measured voltages and currents were scaled into the per-unit system with the control parameters given in Table II were used for the simulation and experiments. The discrete-time PI controller (see 1a) in the dq frame was implemented using the backward difference approximation whereas the MR controller (see 1c) was discretized and implemented using the forward and backward Euler method. The PMR controller (see 1d) was carefully discretized using the Tustin approximation [16]. The reference signals $V_{\alpha,ref}$ and $V_{\beta,ref}$ are the input signals to the SVM to generate the control signals. The 12-bit digital to analog converter (DACs) was used to show the internal signals on the oscilloscope. The inverter was tested under resistive load with the step-change in the load and highly rectifier load as shown in Fig. 7. Fig. 8a shows the simulated dynamic response of the three-phase inverter with an *LC* filter employing

Table III: Experimental data of the inverter

under the rectifier load				
Control schemes	V_o [V]	THD$_v$ [%]	I_o [A]	THD$_i$ [%]
PI	40	28	10	16
PI-MR	40	28	10	2.54
PR-MR	40	28	10	2.40
PMR-MR	40	28	10	0.55
under the *RC* load				
PI	130	0.78	10	1.44
PI-MR	130	0.47	10	0.74
PR-MR	130	0.40	10	0.71
PMR-MR	130	0.24	10	0.38
under the resistive load				
PI	153	0.67	12	0.67
PI-MR	153	0.48	12	0.47
PR-MR	153	0.47	12	0.45
PMR-MR	153	0.36	12	0.33

standard PI controller in a dq frame where Fig. 8b depicts the experimental results. A 10Ω resistive load is connected in parallel to R_d where a step change in the load happens from full load to half load at 0.25s and 0.085s in the simulation and experiment respectively, where the smooth transition happens in the base currents of 10A as shown in Fig. 8. The reference currents in per-unit are 0.7A of the base current I_B. Fig. 9 presents the simulated and experimental implementation of the PI-MR controller under highly nonlinear load. Fig. 10 depicts the discrete implementation of the modified PMR controller where a highly nonlinear load is connected to the inverter. The modified PMR controller in the αβ frame shown in Fig. 10a (simulation) and Fig. 10b (experimental) has superior transient performance compared to the standard PI and PI-MR control in the dq frame. It is evident that the modified PMR controller discretized with Tustin has better harmonic damping capability compared to PI-MR controller. Table III outlines the RMS and the THD values of the output voltage and current for different control schemes. Table III illustrates the effective performance of the PMR-MR controller over the traditional PI, PI-MR, and PR-MR control schemes for resistive, *RC*, and rectifier loads.

Conclusion

This paper explores the harmonic damping schemes of the three-phase inverter for off-grid renewable energy and grid-connected systems. The comparison of the standard current control employing PI and PI-MR control is compared with the proposed modified PMR control supplying linear and highly nonlinear loads. A step-by-step design procedure of the current control loop for the PI-MR and PMR control is presented. The ideal PR control in the αβ frame is equivalent to the PI control in the dq frame. A multi-resonant (MR) controller in the αβ frame with the harmonic components of 5th, 7th, 11th, and 13th, are added in parallel to the fundamental PI controller in the dq frame. The proposed modified PMR controller in αβ frame with the harmonic components of 5th, 7th, 11th, and 13th added to the fundamental controller for the mitigation of the harmonics in the load currents. A proper design methodology of the controllers, system stability analysis, and dynamic and transient performance with the proper methods of discretization are the key points of this paper. The proposed controller offers better dynamic performance, a higher stability margin, ease of digital implementation, and is capable to suppress the load current harmonics with zero-steady state error. The output currents show a lower total harmonic distortion of 0.55 % with the load voltage total harmonic distortion of 28 %. It is found that the proposed modified PMR controller offers fast dynamic and transient performance, good tracking accuracy, and better disturbance rejection under linear and nonlinear loads.

References

[1] F. Blaabjerg, Z. Chen and S. B. Kjaer, "Power electronics as efficient interface in dispersed power generation systems," IEEE Transactions on Power Electronics, vol. 19, no. 5, pp. 1184-1194, 2004.

[2] A. A. Nazeri, P. Zacharias, F. M. Ibanez and I. Idrisov, "Paralleled Modified Droop-Based Voltage Source Inverter for 100% Inverter-Based Microgrids," 2021 IEEE Industry Applications Society Annual Meeting (IAS), 2021, pp. 1-8, 2021.

[3] A. Ali, P. Shanmugham and S. Somkun, "Single-phase grid-connected voltage source converter for LCL filter with grid-current feedback," 2017 International Electrical Engineering Congress (iEECON), 2017, pp. 1-6, 2017.

[4] S. Yang, P. Wang, Y. Tang and L. Zhang, "Explicit Phase Lead Filter Design in Repetitive Control for Voltage Harmonic Mitigation of VSI-Based Islanded Microgrids," IEEE Transactions on Industrial Electronics, vol. 64, no. 1, pp. 817-826, 2017.

[5] D. Chen, J. Zhang and Z. Qian, "An Improved Repetitive Control Scheme for Grid-Connected Inverter With Frequency-Adaptive Capability," IEEE Transactions on Industrial Electronics, vol. 60, no. 2, pp. 814-823, 2013.

[6] R. Wai, C. Lin, Y. Huang and Y. Chang, "Design of High-Performance Stand-Alone and Grid-Connected Inverter for Distributed Generation Applications," IEEE Transactions on Industrial Electronics, vol. 60, no. 4, pp. 1542-1555, 2013.

[7] S. Somkun, "High performance current control of single-phase grid-connected converter with harmonic mitigation, power extraction and frequency adaptation capabilities," IET Power Electronics, vol. 14, no. 2, pp. 352–372, 2021.

[8] A. A. Nazeri, P. Zacharias, F. M. Ibanez and S. Somkun, "Design of Proportional-Resonant Controller with Zero Steady-State Error for a Single-Phase Grid-Connected Voltage Source Inverter with an LCL Output Filter," 2019 IEEE Milan PowerTech, pp. 1-6, 2019.

[9] N. M. Abdel-Rahim and J. E. Quaicoe, "Analysis and design of a multiple feedback loop control strategy for single-phase voltage-source UPS inverters," IEEE Transactions on Power Electronics, vol. 11, no. 4, pp. 532-541, 1996.

[10] D. N. Zmood and D. G. Holmes, "Stationary frame current regulation of PWM inverters with zero steady-state error," IEEE Transactions on Power Electronics, vol. 18, no. 3, pp. 814-822, 2003.

[11] Francis, Bruce A., and William M. Wonham. "The internal model principle for linear multivariable regulators, Applied mathematics and optimization," vol. 2, no. 2, pp. 170-194, 1975.

[12] S. Kouro, P. Cortes, R. Vargas, U. Ammann and J. Rodriguez, "Model Predictive Control—A Simple and Powerful Method to Control Power Converters," IEEE Transactions on Industrial Electronics, vol. 56, no. 6, pp. 1826-1838, 2009.

[13] Somkun, Sakda. "Unbalanced synchronous reference frame control of singe-phase stand-alone inverter." International Journal of Electrical Power & Energy Systems, vol. 107, pp. 332-343, 2019.

[14] M. Liserre, R. Teodorescu and F. Blaabjerg, "Multiple harmonics control for three-phase grid converter systems with the use of PI-RES current controller in a rotating frame," IEEE Transactions on Power Electronics, vol. 21, no. 3, pp. 836-841, 2006.

[15] A. Roshan, R. Burgos, A. C. Baisden, F. Wang and D. Boroyevich, "A D-Q Frame Controller for a Full-Bridge Single Phase Inverter Used in Small Distributed Power Generation Systems," APEC 07 - Twenty-Second Annual IEEE Applied Power Electronics Conference and Exposition, pp. 641-647, 2007.

[16] Teodorescu, Remus, Frede Blaabjerg, Marco Liserre, and P. Chiang Loh. "Proportional-resonant controllers and filters for grid-connected voltage-source converters." IEE Proceedings-Electric Power Applications, vol. 153, no. 5, 750-762, 2006.

[17] A. G. Yepes, F. D. Freijedo, J. Doval-Gandoy, Ó. López, J. Malvar and P. Fernandez-Comesaña, "Effects of Discretization Methods on the Performance of Resonant Controllers," IEEE Transactions on Power Electronics, vol. 25, no. 7, pp. 1692-1712, 2010

[18] D. G. Holmes, T. A. Lipo, B. P. McGrath and W. Y. Kong, "Optimized Design of Stationary Frame Three Phase AC Current Regulators," IEEE Transactions on Power Electronics, vol. 24, no. 11, pp. 2417-2426, 2009.